Biological Psychiatry: Celebrating 50 Years

Archival Report

Mesenchymal Stromal Cells Modulate Peripheral Stress-Induced Innate Immune Activation Indirectly Limiting the Emergence of Neuroinflammation-Driven Depressive and Anxiety-like Behaviors

Denis Gallagher, Fyyaz Siddiqui, Joseph Fish, Maxwell Charlat, Emaan Chaudry, Siddiq Moolla, Andrée Gauthier-Fisher, and Clifford Librach

ABSTRACT

BACKGROUND: Hyperactivation of innate immunity has been implicated in the etiology of mood disorders, including major depressive disorder (MDD). Mesenchymal stromal cells (MSCs) have demonstrated potent immunomodulatory capabilities in the context of chronic inflammatory disease and injury but have yet to be evaluated in stress-based preclinical models of MDD. We sought to test the ability of intravenous MSCs to modulate innate immune activation and behavioral patterns associated with repeated social defeat (RSD).

METHODS: Murine RSD-induced innate immune activation as well as depressive and anxiety-like behaviors were assessed in unstressed, RSD, and RSD + human MSC groups. Biodistribution and fate studies were performed to inform potential mechanisms of action.

RESULTS: MSCs reduced stress-induced circulating proinflammatory cytokines, monocytes, neuroinflammation, and depressive and anxiety-like behaviors. Biodistribution analyses indicated that infused MSCs distributed within peripheral organs without homing to the brain. Murine neutrophils targeted MSCs in the lungs within hours of administration. MSCs and recipient neutrophils were cleared by recipient macrophages promoting a switch toward a regulatory phenotype and systemic resolution of inflammation.

CONCLUSIONS: Peripheral delivery of MSCs modulates central nervous system inflammatory processes and aberrant behavioral patterns in a stress-based rodent model of MDD and anxiety. Recent studies suggest that host immune cell–mediated phagocytosis of MSCs in vivo can trigger an immunomodulatory cascade, resulting in resolution of inflammation. Our data suggest that similar mechanisms may protect distal organs, including the brain, from systemic, stress-induced proinflammatory spikes and may uncover unexpected targets in the periphery for novel or adjunct treatment for a subset of patients with MDD.

Keywords: Cell therapy, Depression, Immunomodulation, Inflammation, MSCs, Resolution

https://doi.org/10.1016/j.biopsych.2019.07.015

Clinical studies have linked innate immune activation to mood disorders, including major depressive disorder (MDD) (1–5). Psychosocial stress is a risk factor for MDD (6), and the transmission of stress-induced inflammatory mediators to the central nervous system (CNS) has been identified as a driver of behavioral perturbations in stress-based rodent models (7–10). Repeated social defeat (RSD) stress provokes egress of proinflammatory monocytes into circulation as well as increased proinflammatory cytokines (11–14). Stress-induced increases in cytokines and migration of monocytes toward the CNS promote neuroinflammation and likely contribute to depressive and anxiety-like behaviors (8,15). The identification of innate immune hyperactivation in the etiology of MDD raises the possibility of targeting inflammation to improve treatment for a subset of patients (2). Studies based on inhibition of specific proinflammatory mediators have been initiated with mixed results (16). Development of therapeutic approaches promoting resolution of inflammation, rather than chronic inhibition of proinflammatory mediators, may minimize side effects, promote repair, and ultimately promote tolerance in inflammatory conditions (17,18).

Mesenchymal stromal cells (MSCs) possess a remarkable ability to modulate the innate and adaptive immune system and create a tolerogenic environment essential for resolution of inflammation (19–23). Immunomodulatory capabilities of MSCs have prompted clinical trials in severe inflammatory conditions

SEE VIDEO CONTENT ONLINE

 ISSN: 0006-3223

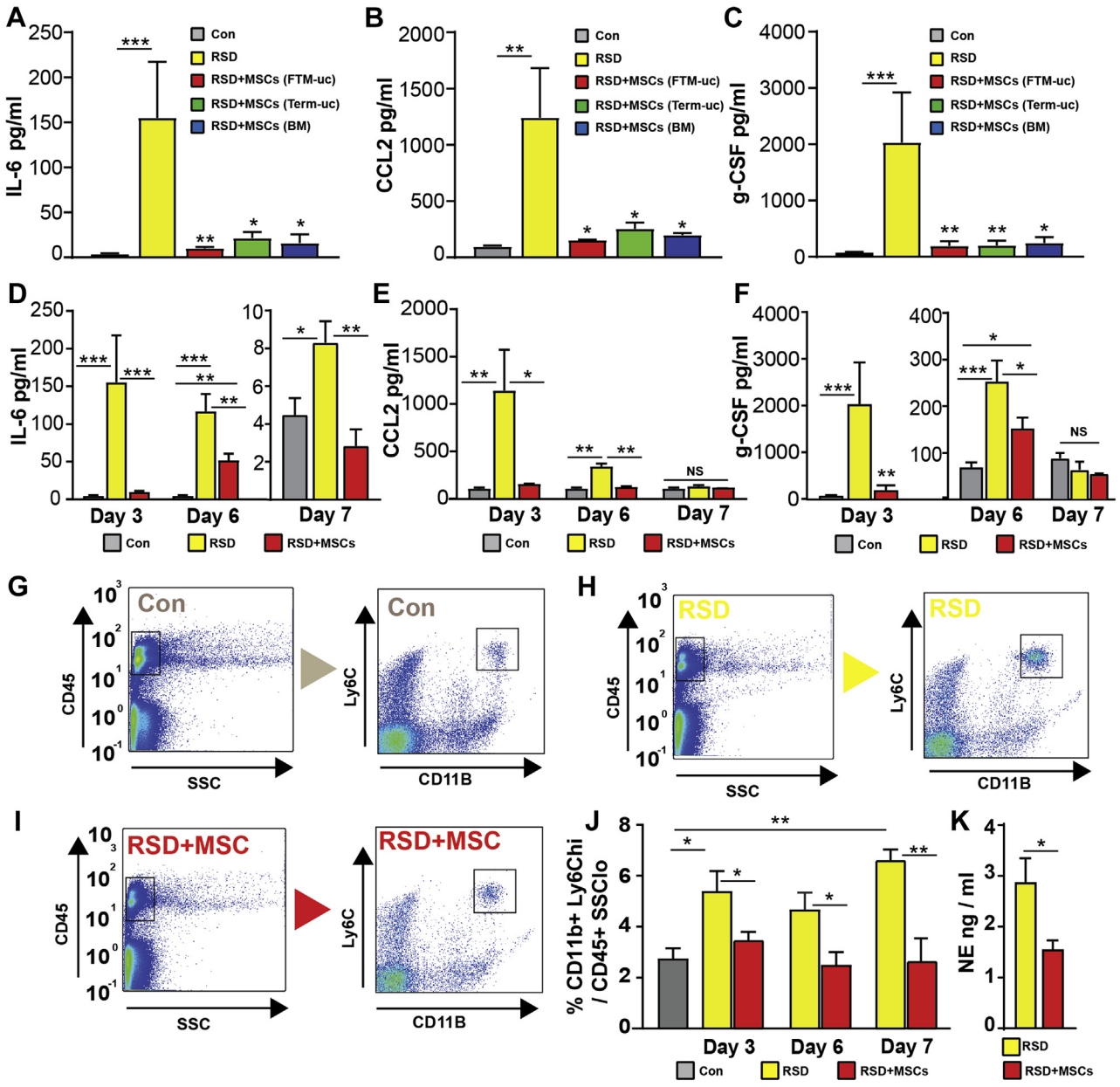

Figure 1. Human mesenchymal stromal cells (MSCs) from multiple sources reduce circulating stress-induced proinflammatory cytokines and Ly6C^{hi} monocytes. **(A–C)** Enzyme-linked immunosorbent assay–quantified plasma concentration of **(A)** interleukin (IL)-6, **(B)** the chemokine CCL2, and **(C)** granulocyte colony-stimulating factor (G-CSF) 20 minutes after cessation of stress on repeated social defeat (RSD) day 3 using MSCs from multiple sources as indicated. **(A)** Control (Con), $n = 19$; RSD, $n = 6$; RSD+MSCs (first-trimester umbilical cord [FTM-uc]), $n = 6$; RSD+MSCs (full-term umbilical cord [Term-uc]), $n = 6$; RSD+MSCs (bone marrow [BM]), $n = 5$. **(B)** Con, RSD, RSD+MSCs (FTM-uc), RSD+MSCs (Term-uc), all $n = 6$; RSD+MSCs (BM), $n = 5$. **(C)** Con, $n = 18$; RSD, $n = 6$; RSD+MSCs (FTM-uc), $n = 6$; RSD+MSCs (Term-uc), $n = 6$; RSD+MSCs (BM), $n = 5$. **(D–F)** Enzyme-linked immunosorbent assay–quantified plasma concentrations of **(D)** IL-6, **(E)** CCL2, and **(F)** G-CSF on RSD days 3, 6 (20 minutes after cessation of RSD), and 7 (20 hours after cessation of RSD). **(D)** Day 6: Con, $n = 19$; RSD, $n = 10$; RSD+MSCs, $n = 8$; Day 7: Con, $n = 19$; RSD, $n = 5$; RSD+MSCs, $n = 5$. **(E)** Day 6: Con, $n = 6$; RSD, $n = 6$; RSD+MSCs, $n = 6$; Day 7: Con, $n = 6$; RSD, $n = 6$; RSD+MSCs, $n = 5$. **(F)** Day 6: Con, $n = 18$; RSD, $n = 14$; RSD+MSCs, $n = 14$; Day 7: Con, $n = 18$; RSD, $n = 5$; RSD+MSCs, $n = 5$. **(G–I)** Representative flow cytometry dot plots from each experimental group showing circulating CD45-positive/SSClo cells as the primary gate and Ly6C^{hi}/CD11b-positive cells as the secondary gate. **(J)** Quantified proportion of circulating Ly6C^{hi}/CD11b-positive cells after cessation of stress on days 3, 6, and 7 (14 hours after session of RSD on day 6) of RSD. **(J)** $n = 4–6$ per group. **(K)** Quantification of circulating norepinephrine (NE) in RSD and RSD+MSCs groups after cessation of stress on day 3 ($n = 6$ per group). Means and error bars representing SEM are shown for all groups, and statistical significance between RSD+Hank's Balanced Salt Solution and RSD+MSCs groups is indicated as $^*p < .05$, $^{**}p < .01$, $^{***}p < .001$, or not significant (NS).

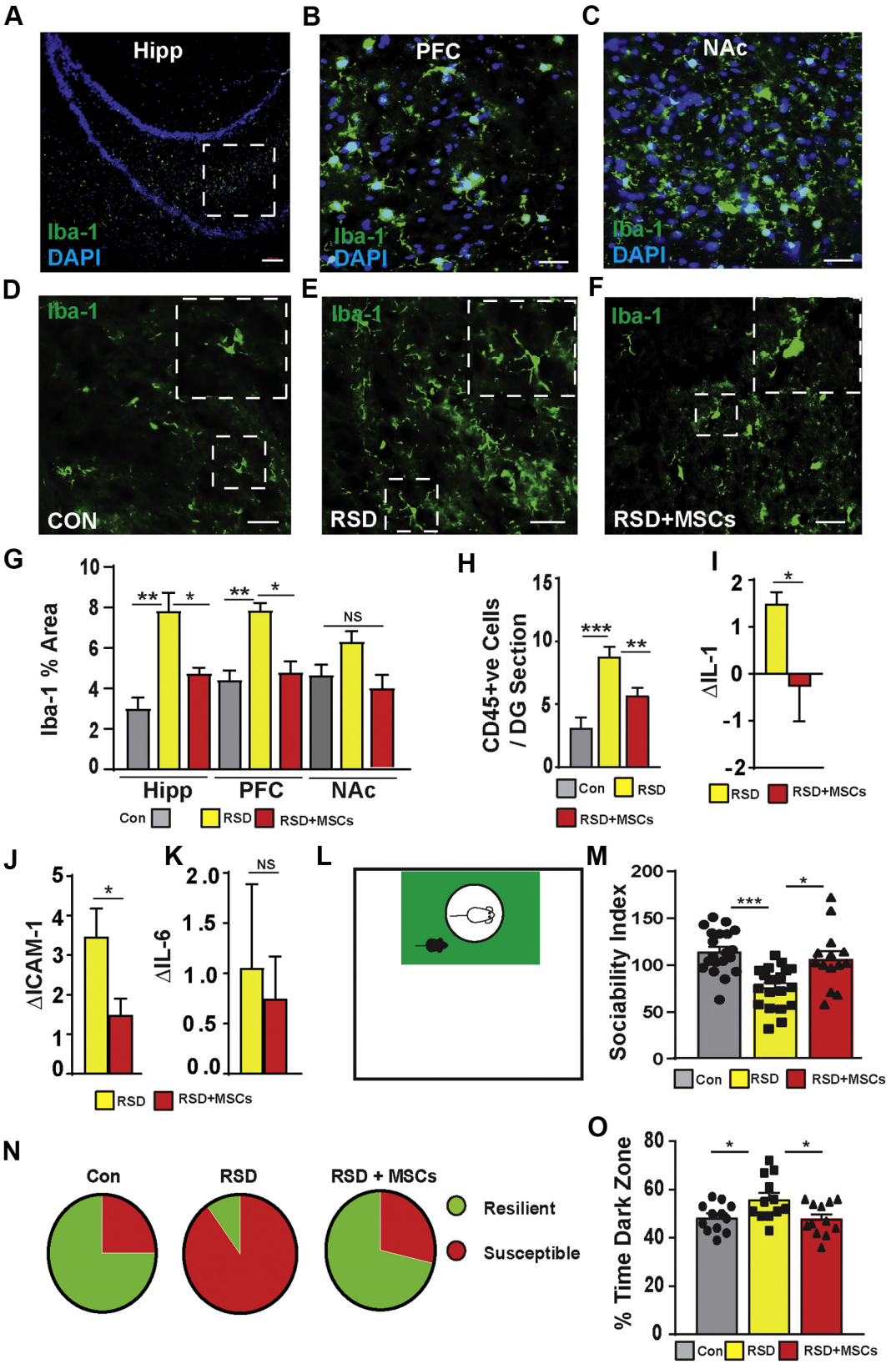
A
Hipp
Iba-1
DAPI
B
PFC
Iba-1
DAPI
C
NAc
Iba-1
DAPI
D
Iba-1
CON
E
Iba-1
RSD
F
Iba-1
RSD+MSCs
G
Iba-1 % Area
Hipp
PFC
NAc
Con
RSD
RSD+MSCs
H
CD45+ve Cells / DG Section
Con
RSD
RSD+MSCs
I
ΔIL-1
RSD
RSD+MSCs
J
ΔICAM-1
RSD
RSD+MSCs
K
ΔIL-6
NS
L
M
Sociability Index
Con
RSD
RSD+MSCs
N
Con
RSD
RSD + MSCs
Resilient
Susceptible
O
% Time Dark Zone
Con
RSD
RSD+MSCs

such as septic shock as well as conditions in which inflammation contributes to pathogenesis, including cardiovascular, autoimmune, and neurodegenerative diseases (20,24,25). However, the widely demonstrated immunomodulatory capabilities of intravenously delivered MSCs have yet to be evaluated in stress-based preclinical models of mood disorders, in which aberrant communication between the immune system and brain promotes depressive and anxiety-like behavioral patterns (9).

Our objectives were to test the ability of intravenous MSCs to modulate stress-induced cytokines and Ly6C^{hi} monocytes and to assess their impact on neuroinflammation and depressive and anxiety-like behaviors (Figures 1 and 2). Despite widespread use in preclinical and clinical studies, questions remain regarding the mechanism of action of MSCs (24,25). Preclinical studies have demonstrated long-lasting therapeutic benefits of MSCs without long-term engraftment, or homing of MSCs to relevant target organs (26,27). Intravenous MSCs have neuroprotective capabilities (28), but efficiency of homing toward the brain is often low, nondetectable, or not reported. MSC-based immunomodulation has largely been attributed to an active paracrine mechanism, involving secretion of anti-inflammatory mediators by MSCs and elicitation of anti-inflammatory responses in recipients (21,29). Recently, an alternative, passive mechanism has been proposed involving clearance of infused MSCs by recipient immune cells, provoking a switch toward anti-inflammatory immune responses (30,31). We sought to determine biodistribution, engraftment, fate, and interaction with recipient innate immune cells as outlined in Supplemental Figure S1 to elucidate potential cellular mechanisms of action.

METHODS AND MATERIALS

Ethics Approval and Consent to Participate

Independent research ethics board approval was obtained for the collection of first-trimester and full-term human umbilical cords (REB #28889, University of Toronto, Canada). Written informed consent was obtained for each sample collection. Term newborn cords were collected via a third party (Life Line Stem Cell, New Haven, IN). Human umbilical cords from first-trimester pregnancies (8–12 weeks of gestation) were obtained from consenting patients who underwent elective pregnancy termination at an independent facility. All animal procedures were approved by the Animal Care Committee of the University Health Network (Toronto, Canada).

Cell Sources, Culture, and Administration

MSC lines from human first-trimester and term umbilical cords were established as described previously (32). Bone marrow MSCs were purchased from Lonza (Morristown, NJ), murine MSCs (C57BL/6) were purchased from Cyagen Biosciences (Santa Clara, CA), and human fibroblasts (hs-68 foreskin-derived) were purchased from ATCC (Manassas, VA). Cells were expanded in minimum essential media with alpha modification, 10% fetal bovine serum, and 1% penicillin/streptomycin, all from Gibco (Gaithersburg, MD). Before intravenous administration via tail vein injection, 1×10^6 cells were resuspended in 200 μL of Hank's Balanced Salt Solution (Life Technologies, Burlington, ON, Canada). RSD animals not receiving MSCs received 200 μL of Hank's Balanced Salt Solution as an injection control, and unstressed control animals remained undisturbed as outlined in Supplemental Figure S1.

Animal Studies and RSD

Animal procedures were conducted and reported according to ARRIVE (Animal Research: Reporting of In Vivo Experiments) guidelines and approved by the Animal Care Committee of the University Health Network (Toronto, Canada). All studies were performed with institutional research ethics board approval (AUP 5232.4, University of Toronto, Toronto, Canada). RSD was carried out as described previously (9,13) and as outlined further in Supplemental Methods and Materials.

Quantification of Cytokines and Ly6C^{hi} Monocytes in Circulation and Quantitative Polymerase Chain Reaction

Blood was collected via cardiac puncture from mice anesthetized with isoflurane at indicated time points. Blood was centrifuged at 2500 rpm for 15 minutes, and plasma was isolated for quantification using Quantikine enzyme-linked immunosorbent assay kits (R&D Systems, Inc., Minneapolis, MN) targeting murine interleukin (IL)-6, the chemokine CCL2, granulocyte colony-stimulating factor (G-CSF), and transforming growth factor β (TGFβ). Lipoxin A4 was quantified via enzyme-linked immunosorbent assay (Aviva Systems Biology, San Diego, CA). Cell pellets were processed according to manufacturer's instructions using Lympholyte-Mammal (Cedarlane, Burlington, ON, Canada) to isolate viable, trypan blue–negative and 7-aminoactinomycin D–negative leukocytes, and the proportion of Ly6C^{hi} monocytes was quantified by flow cytometry as outlined in Supplemental Methods and

Figure 2. Mesenchymal stromal cells (MSCs) reduce central nervous system inflammatory processes and limit depressive and anxiety-like behaviors. **(A–C)** Representative images showing positive ionized calcium-binding adapter molecule 1 (Iba-1) immunostaining of microglia in the proximal CA3 region of the hippocampus (Hipp), the prefrontal cortex (PFC), and the nucleus accumbens (NAc) 20 hours following cessation of repeated social defeat (RSD) (day 7). **(D–F)** Representative images showing positive Iba-1 immunostaining of microglia in the CA3 region of the hippocampus from control (Con) **(D)**, RSD **(E)**, and RSD+MSCs **(F)** groups. **(G)** Quantification of Iba-1–positive area for all groups in Hipp, PFC, and NAc, $n = 4$ per group (scale bar = 50 μm). **(H)** Quantification of CD45-positive cells/field in the dentate gyrus (DG) for all groups, $n = 4$ (scale bar = 50 μm). **(I–K)** Quantitative polymerase chain reaction from whole hippocampus depicting fold change in gene expression relative to normalized unstressed control animals for RSD and RSD+MSCs groups for **(I)** interleukin (*Il*)-1, **(J)** intercellular adhesion molecule 1 (*Icam-1*), and **(K)** *Il-6*, $n = 4$–7 per group. **(L)** Illustration identifying the designated interaction zone used to quantify sociability index (time spent within interaction zone with target CD1 present/time spent in interaction zone without target CD1 × 100). **(M)** Quantification of sociability index for all groups, $n = 14$–21 per group. **(N)** Pie charts representing the proportion of animals per group designated as resilient (sociability index scores 100 or above) or susceptible (sociability index scores less than 100). **(O)** Quantification of percent time spent in the dark chamber of a light/dark box during a test period of 5 minutes, $n = 12$ per group. Means and error bars representing SEM are shown for all groups, and statistical significance between groups is depicted as $^*p < .05$, $^{**}p < .01$, $^{***}p < .001$, or not significant (NS). DAPI, 4′,6-diamidino-2-phenylindole.

Materials. Hippocampus, lung, or leukocytes were isolated from all experimental groups, and gene expression was quantified as outlined in Supplemental Methods and Materials.

Immunohistochemistry, Antibodies, and Microscopy

Mice were transcardially perfused with phosphate-buffered saline, followed by 4% paraformaldehyde. Brains, lungs, and spleens were fixed in 4% paraformaldehyde for 24 hours at 4°C and cryopreserved in 30% sucrose for 24 to 48 hours. Tissues were snap frozen in optimal cutting temperature compound (Electron Microscopy Sciences, Hatfield, PA) and sectioned at 16 to 18 μm. Immunoassays and imaging were carried out as outlined in Supplemental Methods and Materials.

Cell Labeling and Whole-Animal Biodistribution Analyses

Cells were labeled 1 hour before intravenous infusion with Qtracker 625 nanocrystals (Thermo Fisher Scientific, Waltham, MA) according to manufacturer's instructions. Animals were sacrificed in accordance with Animal Care Committee guidelines, immediately embedded in optimal cutting temperature compound and flash frozen in liquid nitrogen. Mice were imaged at 10.23 μm × 10.23 μm in-plane resolution (using an Olympus MVX10 microscope [Olympus Corporation, Tokyo, Japan] with 1× objective and 0.63× magnification) and 40-μm section thickness using the CryoViz cryoimaging system (BioInVision, Inc., Cleveland, OH), further details of which are outlined in Supplemental Methods and Materials.

Statistical Analyses

All plots show mean ± SEM, and statistical significance was assessed using analysis of variance and Tukey's post hoc multiple comparisons analyses comparing experimental groups using GraphPad Prism (GraphPad Software, San Diego, CA). Sample size (*n*) is indicated in figure legends.

RESULTS

MSCs Reduce Circulating Stress-Induced Proinflammatory Cytokines and Monocytes

To test immunomodulation by MSCs in the context of RSD, 1×10^6 MSCs, a dose frequently used in preclinical mouse models (24), from human first-trimester umbilical cord, full-term umbilical cord, or bone marrow, were delivered intravenously on day 2 of RSD as outlined in Supplemental Figure S1. MSCs were characterized using a panel of MSC markers (Supplemental Figure S2). The short-term impact of MSCs on immune activation was assessed following cessation of stress on day 3 of RSD. MSCs decreased circulating levels of RSD-induced innate immune mediators, including IL-6 (Figure 1A), CCL2 (Figure 1B), and G-CSF (Figure 1C). As MSCs from all sources displayed equivalent immunomodulatory capabilities (Figure 1A–C), subsequent studies were undertaken using first-trimester umbilical cord–derived MSCs, a source previously characterized in our laboratory (32). Quantification of cytokines following cessation of RSD on day 6 indicated that MSCs reduced stress-induced proinflammatory mediators several days after infusion (Figure 1D–F). IL-6, but neither CCL2 nor G-CSF, remained elevated in RSD-exposed animals compared with unstressed control mice on day 7, 24 hours after cessation of RSD, and was decreased in animals receiving MSCs (Figure 1D–F). Previous studies have highlighted the importance of stress-induced increases in circulating proinflammatory Ly6C^{hi} monocytes (9,10,12). MSC infusion reduced circulating Ly6C^{hi}, proinflammatory monocytes at days 3, 6, and 7 (Figure 1G–J). RSD-induced increases in circulating monocytes are promoted by norepinephrine, which was also reduced in animals receiving MSCs at the time point during which proinflammatory cytokines are modulated most effectively by MSC, day 3 (Figure 1K). Infusion of MSCs on day 6 of RSD demonstrated moderate modulation of both IL-6 and proinflammatory monocytes quantified on day 7 but was not as effective as early delivery on day 2 (Supplemental Figure S3A, B). Day 2 was used as the infusion time point for subsequent studies. These data demonstrate that MSCs possess immunomodulatory capabilities in the context of stress-induced inflammation.

MSCs Reduce Neuroinflammation and Limit Depressive and Anxiety-like Behaviors

In addition to peripheral innate immune activation in response to stress (Figure 1) (10,12), RSD has been shown to activate microglia and increase trafficking of monocytes/macrophages to the brain, contributing to depressive and anxiety-like behaviors, including increased social avoidance and dark preference (10,13,15,33). Intravenously delivered MSCs have previously demonstrated neuroprotective capabilities following neuronal injury or degeneration (28). Our objective was to test the ability of intravenous MSCs to modulate RSD-induced neuroinflammation and aberrant behavioral patterns. In accordance with previous studies (10,13,15,33), RSD significantly activated microglia as measured by the proportional increases in ionized calcium-binding adapter molecule 1–positive area in the hippocampus, prefrontal cortex, and nucleus accumbens (Figure 2A–F). The extent of RSD-induced microglial activation was lower in animals receiving MSCs compared with RSD-exposed animals not infused with MSCs (Figure 2G). Previous studies have shown increased trafficking of peripherally derived CD45-positive monocytes/macrophages to the hippocampus following RSD (34,35). Animals receiving MSCs showed reduced recruitment of CD45 cells to the hippocampus compared with RSD animals (Figure 2H and Supplemental Figure S4A). Hippocampal gene expression studies quantifying induction of selected proinflammatory mediators revealed significant modulation of RSD-induced *Il-1β* and intercellular adhesion molecule 1 (Figure 2I and J), but not *Il-6* (Figure 2K). Assessment of social interaction and anxiety-like behaviors following RSD has revealed significant stress-associated behavioral perturbations (8,15). Decreased sociability and increased anxiety following RSD are thought to be driven by increases in both systemic and CNS inflammatory processes (7). We next sought to test the ability of MSCs to regulate social avoidance and anxiety-like behaviors. RSD has been shown to reduce sociability, as quantified by a reduction in time spent in close proximity to an unfamiliar mouse within a designated interaction zone as illustrated in Figure 2L, a behavioral pattern we also observed in RSD-exposed mice

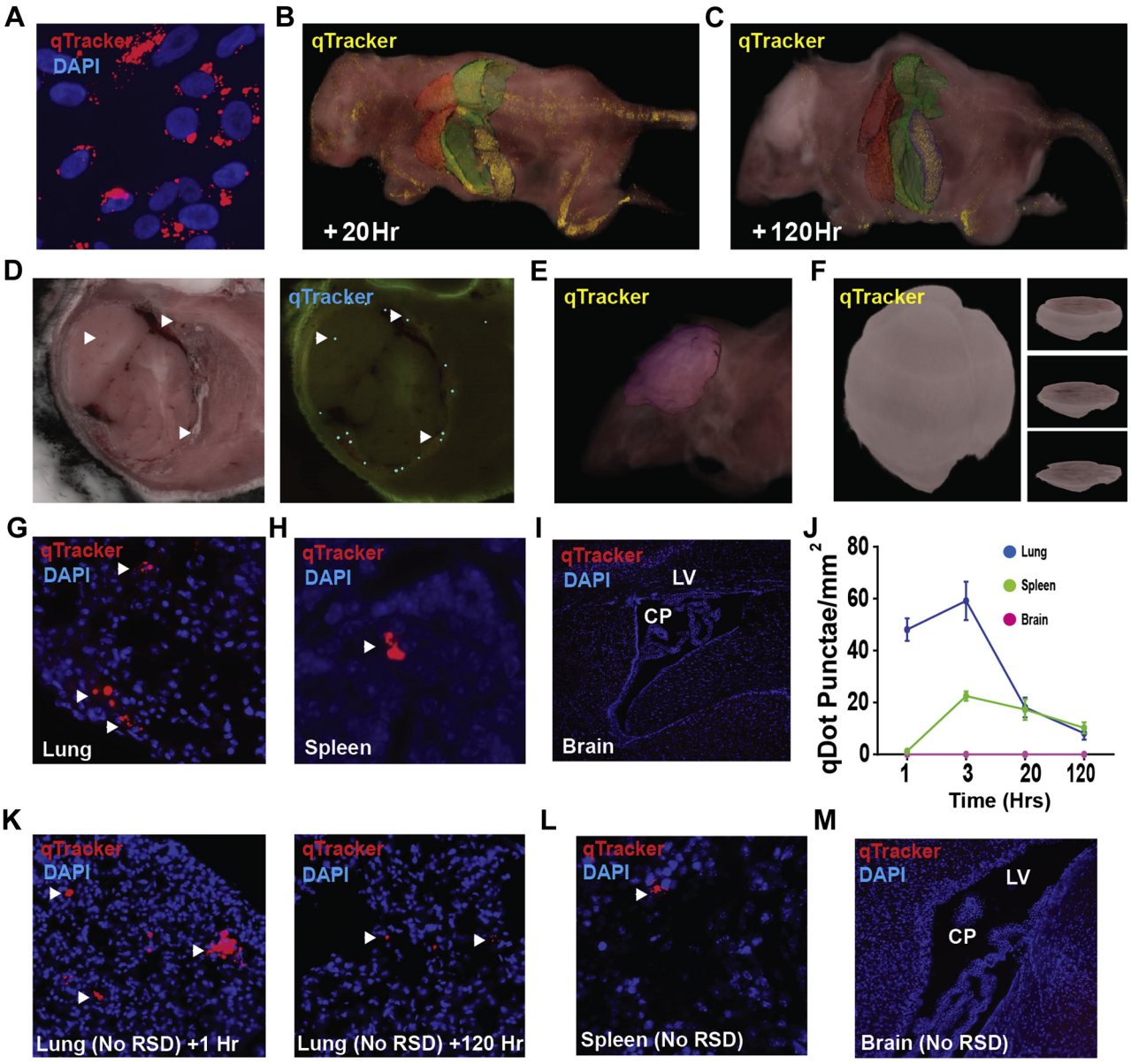

Figure 3. Mesenchymal stromal cells (MSCs) are distributed peripherally and do not home to the brain during repeated social defeat (RSD). **(A)** Representative image demonstrating efficient uptake of Qtracker 625 nanocrystals (red) to MSCs (4′,6-diamidino-2-phenylindole [DAPI]/blue) in vitro before intravenous administration (scale bar = 20 μm). **(B, C)** Three-dimensional reconstruction from serial whole-animal cryosections depicting primary anatomical locations of Qtracker 625 punctae (pseudo-colored yellow) 20 hours **(B)** and 120 hours **(C)** following intravenous administration of Qtracker 625–labeled MSCs. See Supplemental Videos 1 and 2. **(D)** Representative bright-field image (left panel) and corresponding fluorescent image with occasional Qtracker 625 punctae in the meninges highlighted blue (right panel). **(E)** Three-dimensional reconstruction focused on the brain with Qtracker 625 and **(F)** three-dimensional reconstruction (left panel) and representative optical slices through the brain of animals receiving Qtracker 625–labeled MSCs showing little or no detectable signal; see Supplemental Video 3. Representative image of immunohistochemical staining of **(G)** lungs, **(H)** spleen, and **(I)** brain 20 hours following intravenous administration of Qtracker 625–labeled (red) MSCs (scale bar = 50 μm). **(J)** Immunohistochemistry-based quantification of Qtracker 625 punctae/mm^2 in lung (blue), spleen (green), and brain (pink) at several time points following intravenous infusion of Qtracker 625–labeled MSCs, n = 3 per group. **(K–M)** Representative images demonstrating the same biodistribution pattern of Qtracker 625–labeled MSCs injected into unstressed control animals with cells readily detected in lung **(K)** and spleen **(L)** but not within brain **(M)**. CP, choroid plexus; LV, lateral ventricle.

(Figure 2M). MSC infusion into RSD-exposed or unstressed (Supplemental Figure S4B, C) mice was associated with social interaction indices and proportions of resilient (social interaction indices above 100) animals similar to unstressed control animals (Figure 2M, N). Late infusion of MSCs on day 6 of RSD also improved sociability but did not reach statistical significance thresholds (Supplemental Figure S4D, E). RSD has also been shown to provoke increased dark preference in the light/dark preference test of anxiety-like behavior (Figure 2O). MSC infusion was associated with moderately decreased dark

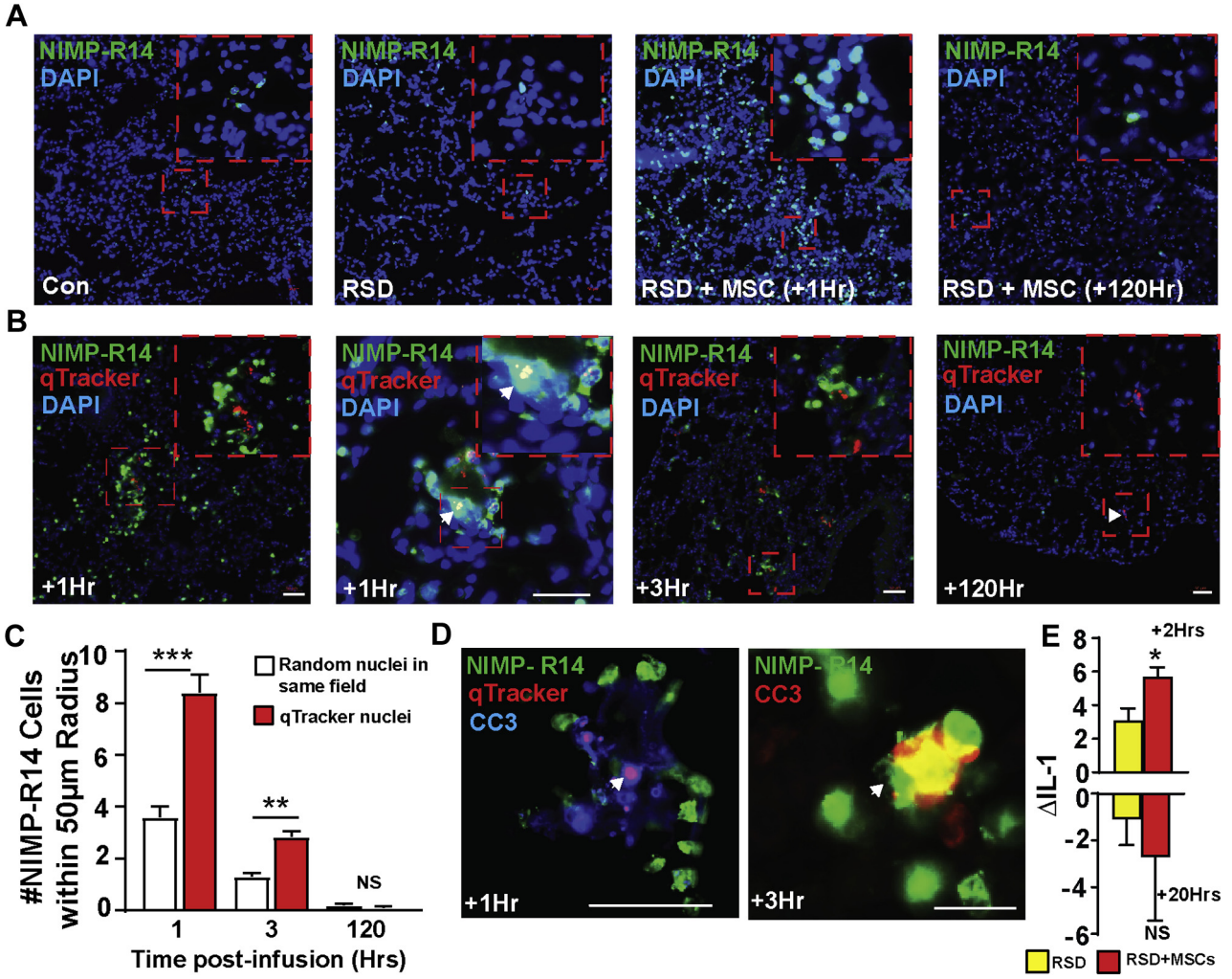

Figure 4. Mesenchymal stromal cells (MSCs) transiently recruit recipient innate immune cells to the lung. **(A)** Representative images of lung cryosections immunostained with an anti-murine neutrophil antibody, NIMP-R14 (green) in control (Con), repeated social defeat (RSD), and RSD+MSC at indicated time points following administration of MSCs (scale bar = 50 μm). **(B)** Representative images of Qtracker 625–positive punctae (red) in the lungs surrounded by (first panel from left) or completely engulfed by (second panel from left/inset) murine recipient neutrophils (green) within 1 hour of intravenous infusion of Qtracker 625–labeled MSCs. By 120 hours after administration (far right panel), murine neutrophils (green) were decreased in number and no longer associated with remaining Qtracker 625–positive punctae (scale bar = 50 μm). **(C)** Quantification of the number of NIMP-R14-positive neutrophils within a 50-μm radius of either Qtracker 625–positive punctae or randomly selected nuclei within the same field, $n = 4$ per time point, 100–150 nuclei analyzed per animal. Means and error bars representing SEM are shown for all time points, and statistical significance between Qtracker 625–positive punctae and randomly selected nuclei within the same field is indicated as $^{**}p < .01$, $^{***}p < .001$, or not significant (NS). **(D)** Representative image displaying Qtracker 625–positive punctae (red) colocalized with increased cleaved caspase 3 (CC3) (blue) and surrounded by NIMP-R14-positive neutrophils (green) 1 hour following intravenous infusion of Qtracker 625–labeled MSCs (left panel) and apoptotic (CC3) (red), NIMP-R14-positive murine neutrophils (green) 3 hours following administration of MSCs (right panel) (scale bar = 50 μm). **(E)** Quantitative polymerase chain reaction from whole-lung tissue displaying fold increase (top) or decrease (bottom) of interleukin *(Il)-1* gene expression relative to unstressed control animals at 2 hours (top) and 20 hours (bottom) following MSC infusion. DAPI, 4′,6-diamidino-2-phenylindole.

preference (Figure 2O) compared with RSD-exposed animals not receiving cells. These data suggest that intravenous delivery of MSCs during stress reduce neuroinflammation and stress-induced behavioral perturbations commonly quantified using this model.

MSCs Are Distributed Peripherally and Do Not Home to the Brain During RSD

Both systemic and CNS innate immune activation in response to stress are dampened by intravenous MSCs (Figures 1 and 2). To help determine whether immunomodulatory effects on the CNS were the result of active MSCs homing toward the brain, biodistribution studies were undertaken following infusion. Qtracker 625–labeled MSCs (Figure 3A) were delivered intravenously to stressed mice, and whole-animal cryoimaging was performed to identify primary sites of MSC engraftment. MSCs distributed almost entirely among peripheral tissues, including the lung, liver, and spleen, at 20 hours (Figure 3B and Supplemental Video 1) and 120 hours (Figure 3C and Supplemental Video 2) following infusion. Qtracker 625–

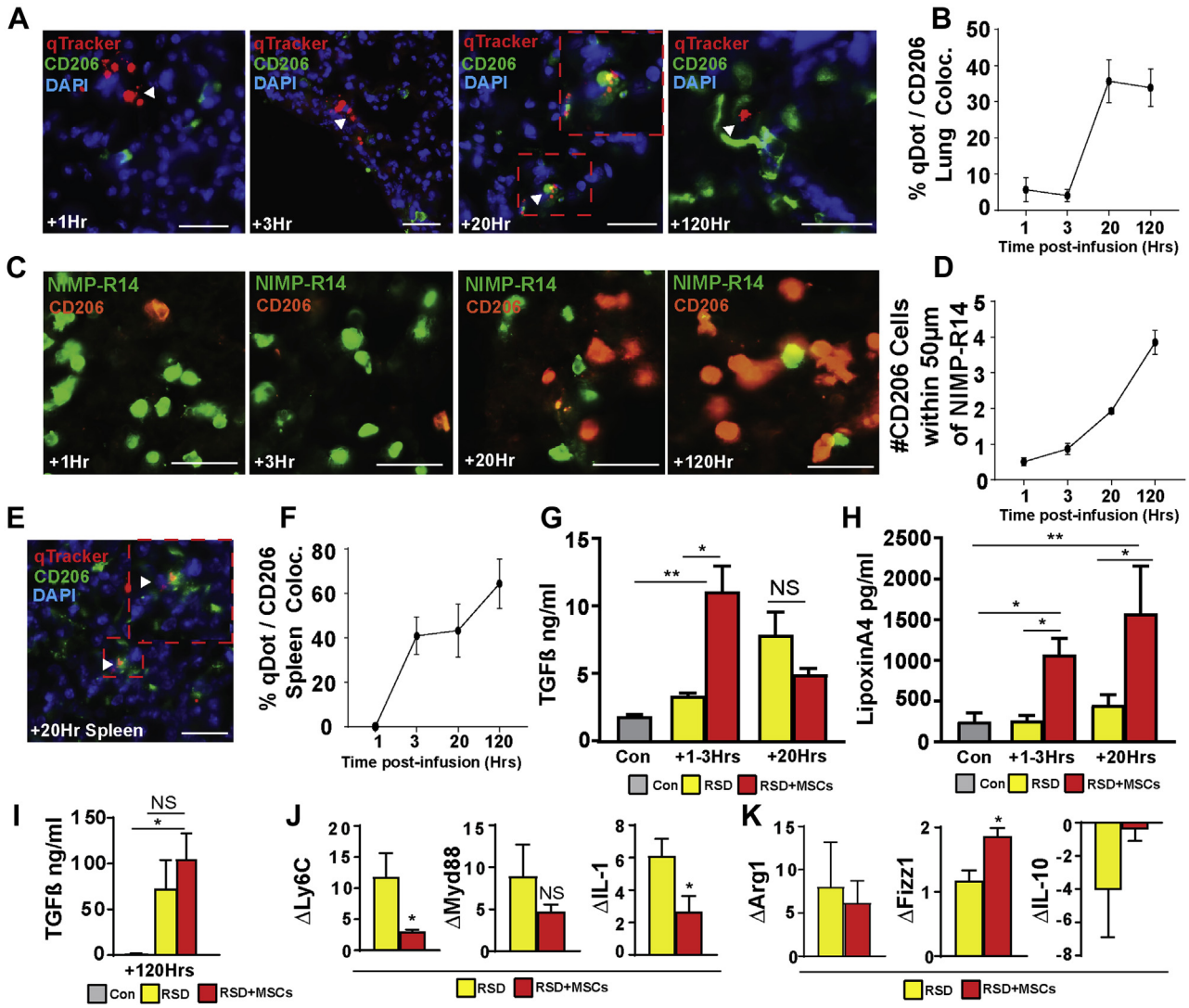

Figure 5. Mesenchymal stromal cells (MSCs) and recruited recipient innate immune cells are targeted by recipient macrophages promoting resolution of inflammation. **(A)** Representative images displaying CD206-positive M2 macrophages (green) in the lungs at 1, 3, 20, and 120 hours following intravenous infusion of Qtracker 625–labeled MSCs (red) and engulfment and colocalization of Qtracker 625–labeled MSCs by CD206-positive macrophages at +20 and +120 hours. **(B)** Quantification of percent Qtracker 625–positive punctae colocalized with CD206-positive recipient macrophages at indicated time points, $n = 4$ per time point. **(C)** Representative images showing recruitment of CD206-positive macrophages (orange) to areas containing recipient neutrophils (green) at 20 and 120 hours following MSC infusion. **(D)** Quantification of the number of CD206-positive macrophages within a 50-µm radius of NIMP-R14-positive neutrophils at each indicated time point, $n = 4$ per time point with 100–150 cells sampled per animal. **(E)** Representative image displaying engulfment and colocalization of Qtracker 625–labeled MSCs (red) by CD206-positive macrophages (green) at 120 hours in the spleen and **(F)** quantification of the percent Qtracker-positive punctae colocalized with CD206-positive macrophages in the spleen throughout repeated social defeat (RSD), $n = 4$ per experimental group (scale bars = 50 µm). **(G)** Enzyme-linked immunosorbent assay–quantified plasma concentrations of transforming growth factor β (TGFβ) in control (Con) (gray bar), RSD (yellow bar), and RSD+MSCs (red bar) at indicated time points following infusion of MSCs. Con, $n = 5$; RSD + 1–3 hours, $n = 5$; RSD+MSCs + 1–3 hours, $n = 9$; RSD + 20 hours, $n = 5$; RSD+MSCs + 20 hours, $n = 5$. **(H)** Enzyme-linked immunosorbent assay–quantified plasma concentrations of lipoxin A4 in Con (gray bar), RSD (yellow bar), and RSD+MSCs (red bar) at indicated time points following infusion of MSCs. Con, $n = 7$; RSD + 1–3 hours, $n = 6$; RSD+MSCs + 1–3 hours, $n = 9$; RSD + 20 hours, $n = 3$; RSD+MSCs + 20 hours, $n = 3$. **(I)** Enzyme-linked immunosorbent assay–quantified plasma concentrations of TGFβ in Con (gray bar), RSD (yellow bar), and RSD+MSCs (red bar) at 120 hours following MSC infusion (14 hours after cessation of final RSD session). Con, $n = 5$; RSD, $n = 5$; RSD+MSCs, $n = 6$. Quantitative polymerase chain reaction from isolated leukocytes displaying fold increase or decrease of indicated proinflammatory **(J)** and anti-inflammatory **(K)** genes following cessation of stress on day 3, $n = 3$–4 per group. Means and error bars representing SEM are shown for all groups, and statistical significance between indicated groups is depicted as $^{*}p < .05$, $^{**}p < .01$, or not significant (NS). DAPI, 4′,6-diamidino-2-phenylindole.

positive punctae were occasionally detected in the meninges (Figure 3D), but MSC engraftment within the CNS parenchyma was either nondetectable or negligible following infusion (Figure 3E, F and Supplemental Video 3). Immunohistochemical analyses confirmed whole-animal observations, with Qtracker 625–positive punctae readily detectable in lung

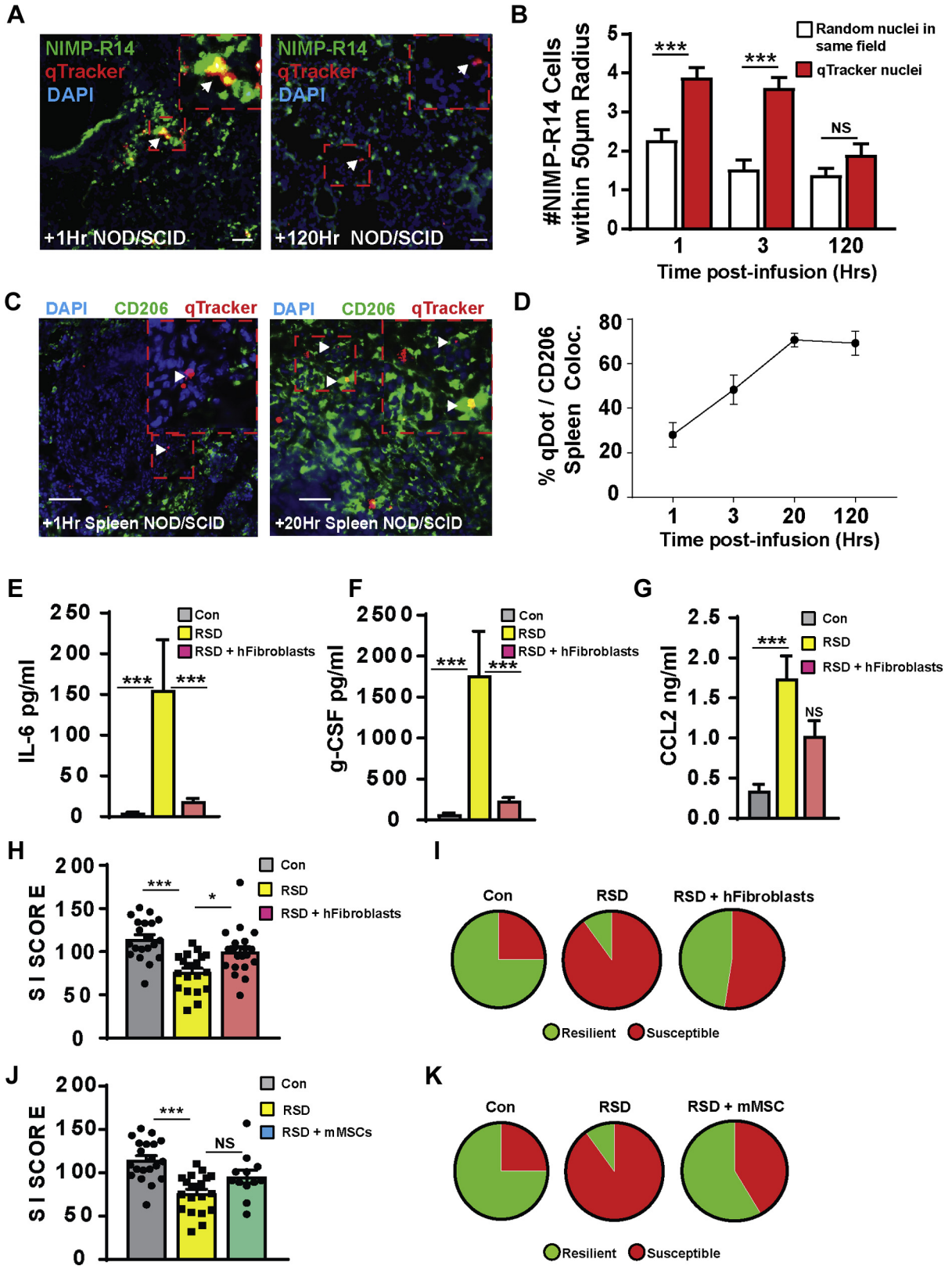
A
NIMP-R14
qTracker
DAPI
+1Hr NOD/SCID
NIMP-R14
qTracker
DAPI
+120Hr NOD/SCID
B
#NIMP-R14 Cells within 50µm Radius
Random nuclei in same field
qTracker nuclei
***
***
NS
1
3
120
Time post-infusion (Hrs)
C
DAPI CD206 qTracker
DAPI CD206 qTracker
+1Hr Spleen NOD/SCID
+20Hr Spleen NOD/SCID
D
% qDot / CD206 Spleen Coloc.
1
3
20
120
Time post-infusion (Hrs)
E
IL-6 pg/ml
Con
RSD
RSD + hFibroblasts
F
g-CSF pg/ml
G
CCL2 ng/ml
NS
H
SI SCORE
I
Con
RSD
RSD + hFibroblasts
Resilient
Susceptible
J
SI SCORE
RSD + mMSCs
K
RSD + mMSC

(Figure 3G, J) and spleen (Figure 3H, J), but not in brain (Figure 3I, J). The number of Qtracker 625–positive punctae steadily decreased following administration (Figure 3B, C, J), suggesting that MSCs are cleared from recipients during RSD. To rule out the possibility that biodistribution of MSCs is influenced by RSD, labeled MSCs were injected into unstressed control animals, revealing the same biodistribution pattern in the lung (Figure 3K) and spleen (Figure 3L) at multiple time points and not the CNS (Figure 3M). This biodistribution pattern suggests that CNS immunomodulatory and behavioral improvements associated with intravenous MSCs are not the result of active homing of infused cells to the brain.

MSCs Transiently Recruit Recipient Innate Immune Cells to the Lung

Previous studies as well as our own observations in the RSD model (Figure 3) have demonstrated that intravenously delivered MSCs become trapped in the lungs within minutes of administration (26,27). To investigate the fate of infused MSCs and shed light on potential mechanisms by which infused cells modulate innate immunity, we examined the interaction between Qtracker 625–prelabeled MSCs and recipient mouse innate immune cells in the lungs covering the duration of RSD. As neutrophils and monocytes are often the first innate immune cell to respond to injury or infection (36,37), we assessed their recruitment to the lung using a highly murine-specific antibody often used to detect or deplete neutrophils (NIMP-R14) (38–40), which recognizes Ly6G (predominantly expressed on neutrophils) and Ly6C (expressed on some monocyte populations). Immunohistochemical analyses revealed rapid and transient recruitment of neutrophils and monocytes to the lungs within 1 hour of MSC administration, which was not observed in unstressed control animals or RSD animals (Figure 4A). To confirm that recipient neutrophils and monocytes were recruited to the lungs as a direct result of MSC infusion, analyses investigating colocalization of NIMP-R14–positive cells with Qtracker 625–positive punctae were undertaken following intravenous infusion (Figure 4B). Before infusion, MSCs displaying Qtracker 625–positive punctae in vitro were completely negative for NIMP-R14 (Supplemental Figure S5A). Within 1 hour of infusion, murine NIMPR-14–positive neutrophils and monocytes rapidly swarmed and often engulfed and completely colocalized with Qtracker 625–labeled MSCs (Figure 4B). At 120 hours post-infusion, after cessation of RSD, detectable Qtracker 625–positive punctae were reduced in the lung (Figures 3C, J and 4B [far right panel]), and remaining neutrophils and monocytes were no longer primarily associated with remaining Qtracker 625–labeled MSCs (Figure 4B). To quantify the association between infused MSCs and recipient innate immune cells, the number of NIMP-R14–positive cells within a 50-μm radius of Qtracker 625–positive punctae were compared with the number of NIMP-R14–positive cells within a 50-μm radius of randomly selected nuclei within the same field as Qtracker 625–positive punctae (Figure 4C). These data revealed that neutrophil recruitment to the lung is rapid, transient, and a direct result of MSC infusion (Figure 4C). Co-immunostaining for cleaved caspase 3 revealed that both infused Qtracker 625–positive MSCs and NIMP-R14–positive cells activate apoptotic pathways within hours of MSC infusion (Figure 4D). These data reveal a rapid and transient proinflammatory response in the lung mediated primarily by recipient neutrophils and monocytes, which correlated with transient increases in lung *Il-1* expression in animals receiving MSCs within 2 hours of administration (Figure 4E).

MSCs and Recruited Recipient Innate Immune Cells Are Targeted by Recipient Macrophages Promoting Resolution of Inflammation

The rate of effective neutrophil clearance, largely carried out by macrophages, is a crucial index of the resolution of inflammation (36,41,42). Phagocytosis of neutrophils by macrophages has been shown to promote a switch from a proinflammatory to an anti-inflammatory macrophage phenotype associated with increased expression of CD206 (43,44). Assessment of CD206-positive macrophages in the lungs following infusion of Qtracker 625–labeled MSCs revealed a significant increase in the number of CD206-positive cells in the lung associated with Qtracker 625–positive punctae at 20 and 120 hours following infusion (Figure 5A, B), an association

Figure 6. Innate immune detection and clearance of infused cells may be a key contributor to associated anti-inflammatory and behavioral effects. **(A)** Representative images of Qtracker 625–positive punctae (red) in the lungs of immunocompromised nonobese diabetic/severe combined immunodeficient (NOD/SCID) mice surrounded and engulfed by recipient murine neutrophils (green) within 1 hour of intravenous infusion of Qtracker 625–labeled mesenchymal stromal cells (MSCs) (left panel). By 120 hours after administration (right panel), murine neutrophils (green) were decreased in number and no longer primarily associated with remaining Qtracker 625–positive punctae (scale bar = 50 μm). **(B)** Quantification of the number of NIMP-R14–positive neutrophils within a 50-μm radius of either Qtracker 625–positive punctae or randomly selected nuclei within the same field, $n = 3$ per time point, 100–150 nuclei analyzed per animal. Means and error bars representing SEM are shown for all time points, and statistical significance between Qtracker 625–positive punctae and randomly selected nuclei within the same field is indicated as $^{***}p < .001$ or not significant (NS). **(C)** Representative image displaying Qtracker 625–punctae (red) and CD206-positive macrophages (green) +1 hour (left panel) and +20 hours (right panel) in the spleen tissue from NOD/SCID mice and **(D)** quantification of the percent Qtracker 625–positive punctae colocalized with CD206-positive macrophages in the spleen of NOD/SCID mice at indicated time points throughout repeated social defeat (RSD), $n = 3$ per experimental group per time point (scale bars = 50 μm). **(E–G)** Enzyme-linked immunosorbent assay–quantified plasma concentration of **(E)** interleukin (IL)-6, **(F)** granulocyte colony-stimulating factor (G-CSF), and **(G)** the chemokine CCL2 20 minutes after cessation of stress on RSD day 3 in control (Con), RSD, and RSD+hs-68-human fibroblasts (hFibroblasts). Statistical significance between RSD and RSD+hFibroblasts is indicated as $^{***}p < .001$ or NS. **(H)** Sociability index (SI) scores were quantified for Con ($n = 20$), RSD ($n = 20$), and RSD + hFibroblasts ($n = 21$) and categorized as susceptible (SI <100) or resilient (SI >100) and presented as pie charts in panel **(I)**. **(J)** SI scores were quantified for Con ($n = 20$), RSD ($n = 20$), and RSD+mouse MSCs (mMSCs) ($n = 12$) and categorized as susceptible (SI <100) or resilient (SI >100) and presented as pie charts in panel **(K)**. Statistically significant differences between RSD and RSD + mMSCs were not detected, as indicated (NS). DAPI, 4′,6-diamidino-2-phenylindole.

not detected at earlier time points (Figure 5A, B). Before infusion, Qtracker 625–labeled MSCs were completely negative for CD206 (Supplemental Figure S5B). CD206-positive cells were also associated with recruited recipient NIMP-R14-positive neutrophils and monocytes at later time points (Figure 5C, D). In contrast to the lung, Qtracker 625–positive punctae were not readily detectable at 1 hour following infusion but accumulated between 3 and 120 hours in the spleen (Figure 5E, F). Analyses of spleen revealed gradual increases in Qtracker 625–positive punctae colocalized with CD206-positive cells during RSD (Figure 5F). Data presented in Figures 3–5 suggest that recruitment of innate immune cells to the lungs following MSC infusion leads ultimately to the clearance of both MSCs and recruited neutrophils and monocytes, processes known to promote active resolution of systemic inflammation and repair (43) that may underlie our observed decreases in circulating proinflammatory cytokines and monocytes (Figure 1). We sought to quantify circulating concentrations of known anti-inflammatory and pro-resolution mediators, including TGFβ and lipoxin A4, following cell infusion. Animals receiving MSCs had significantly elevated circulating concentrations of both TGFβ (Figure 5G) and lipoxin A4 (Figure 5H). Circulating levels of TGFβ on day 7 were not significantly different between RSD and RSD + MSCs groups (Figure 5I), indicating that active increases in anti-inflammatory mediators may be a transient event with longer-lasting effects on proinflammatory responses to subsequent stressors (Figure 1). In that regard, RSD induction of proinflammatory genes, including *Ly6c* (Figure 5J) and *Il-1* (Figure 5J), in circulating leukocytes was reduced at day 3, with MSC-induced modulation of selected anti-inflammatory genes including *Fizz1* and *Il-10* also detected (Figure 5K). These data suggest that MSC infusion initiates a cascade of cellular events starting with innate immune targeting of infused cells and ultimately resulting in the clearance of MSCs and recruited innate immune cells, promoting a switch toward anti-inflammatory or regulatory phenotypes detectable systemically.

Innate Immune Detection and Clearance of Infused Cells May Be a Key Contributor to Associated Anti-inflammatory and Behavioral Effects

To confirm that recognition and clearance of infused MSCs is mediated by the innate immune system, fate-based assays were performed using nonobese diabetic/severe combined immunodeficient (NOD/SCID) mice lacking B and T cells (45,46). Qtracker 625–positive MSCs were rapidly surrounded or engulfed by NIMP-R14-positive recipient NOD/SCID neutrophils and monocytes in the lung (Figure 6A). Quantification of neutrophil swarming revealed a similar pattern to that observed in immunocompetent animals, with neutrophil swarming being readily detectable within hours of administration (Figure 6B), but less at 120 hours postinfusion, indicating significant clearance of both infused cells and recruited neutrophils. Qtracker 625–positive punctae were found to accumulate in the spleen of NOD/SCID mice and associate with CD206-positive cells (Figure 6C, D). To test immunomodulation by a non-MSC cell type, we chose human foreskin-derived fibroblasts and infused them intravenously on day 2 of RSD. Quantification of circulating proinflammatory cytokines on day 3 of RSD, the time point of maximal immune modulation by MSC (Figure 1), revealed that human fibroblasts attenuated RSD-induced increases in IL-6 and G-CSF (Figure 6E, F), but in contrast to infused MSCs, significant reduction of CCL2 was not detected (Figure 6G). Quantification of social avoidance in RSD-exposed animals receiving fibroblasts revealed sociability indices and resilience similar to that of unstressed control animals and significantly higher than RSD-exposed animals (Figure 6H, I). Behavioral assessments using murine MSCs revealed a trend toward improved resilience, but did not reach statistical significance (Figure 6J, K). These data raise the possibility that the extent of innate allo-recognition or xeno-recognition of infused cell types from diverse sources may contribute significantly to their clearance and ultimately their anti-inflammatory and neuroprotective effects, as summarized graphically in Supplemental Figure S6.

DISCUSSION

Therapeutic approaches targeting systemic and CNS inflammation may hinder the initiation or progression of neurological conditions, including MDD (7,47). Results presented here suggest that the well-established immunomodulatory effects of MSCs in the context of infection or injury can be extended to stress-induced inflammation. We show that intravenous infusion of MSCs reduces circulating MDD-associated cytokines, including IL-6 (2,11,48–50). RSD also increases circulating proinflammatory monocytes (10,13,51), a population reduced in animals receiving intravenous MSCs. MSC infusion also limits neuroinflammation and RSD-induced depressive and anxiety-like behaviors. Biodistribution and fate studies demonstrate clearance of MSCs without homing to the brain, suggesting that modulation of neuroinflammation and behavior is a downstream consequence of systemic immunomodulation. Finally, we demonstrate that recipient neutrophils are transiently recruited to the lungs in response to infused cells and that the clearance of infused exogenous cells and recruited recipient neutrophils from the lungs promotes a switch toward a regulatory phenotype in CD206-positive macrophages as well as transiently increased circulating anti-inflammatory mediators.

Injection of MSCs into the CNS has been shown to reduce depressive behaviors in mice following traumatic brain injury (52) and in genetically susceptible rats (53,54). Our study suggests that MSCs also have antidepressant effects in a stress-based model. Importantly, we found that intravenous cell delivery modulates systemic and CNS inflammatory processes and aberrant stress-induced behavioral patterns. Our findings support the emerging concept that chronic stress activates systemic and CNS inflammatory processes and that innate immune mediators may be promising targets for novel or adjunct therapies in at least a subset of patients with MDD (7,16). Targeting specific proinflammatory mediators, including IL-6, has led to promising results in preclinical MDD and anxiety models (55). Translation of similar, targeted approaches to clinical application in patients with MDD has yielded mixed results and suggests that a subset of patients with MDD may be more responsive to anti-inflammatory interventions (7,16). Rather than chronically inhibiting the action of a specific proinflammatory mediator, MSC infusion initiates a cascade of cellular events culminating in moderate downregulation of

multiple proinflammatory mediators. Moderate, multipronged, transient modulation of inflammation and resolution cascades by MSCs may offer advantages over approaches in which individual cytokines are completely ablated in the long term.

The mechanism of action underlying anti-inflammatory properties of MSC in vivo is a subject of ongoing discussion, with evidence supporting both active paracrine mechanisms and a comparatively passive, phagocytosis-driven immunomodulatory pathway (24). Although data presented here do not exclude the contribution of an active, paracrine mechanism of action in the short term, the rapidity of neutrophil recruitment to the lungs and subsequent engulfment and clearance of infused MSCs (Figures 3–5) suggest that a phagocytosis-driven mechanism is more likely to underlie longer-lasting effects. Future work focused on splenic reservoirs of Ly6C^{hi} monocytes may provide further insight into longer-term immunomodulation by MSCs even after they have been cleared from recipients. Phagocytosis-driven immunomodulation outlined in previous studies (30,31) as well as results presented here help explain immunosuppressive effects associated with infusion of apoptotic cells, in which active paracrine mechanisms are, presumably, not implicated. Although less studied, regenerative capabilities have also been attributed to infused, viable, non-MSCs, including fibroblasts in vivo (Figure 6E–I) (56), supporting the possibility that allorejection of infused cells from diverse sources may promote resolution of inflammation.

It is plausible that preclinical benefits associated with cell therapy products, in which initial engraftment is low or incomplete, may be at least partially attributable to enhancement of a cellular resolution cascade similar to that described here. Our preliminary assessment of cell fate in NOD/SCID mice (Figure 6A–D) raises the possibility that human cells, currently being tested in preclinical rodent models, may initially be targeted by recipient innate immune cell populations at very early, often uninvestigated, time points, including neutrophils and monocytes, which persist in commonly used immunocompromised animals lacking T and B lymphocytes (45,46). Similarly, antidepressant activity of MSCs infused directly into the CNS has been attributed to active promotion of neurogenesis via paracrine signaling from infused cells (53,54). However, MSC engraftment following direct infusion into the CNS is reportedly low in these studies, raising the intriguing possibility that regeneration associated with therapeutic cells injected directly into the CNS in preclinical models is at least partially the result of recipient microglia-driven phagocytosis of infused cells, as M2 microglia promote neurogenesis (57).

At the cellular level, neutrophil death and clearance by macrophages has been identified as a critical turning point between inflammation and its resolution (36). The recruitment and subsequent clearance of neutrophils to and from the lung in response to intravenous MSCs may represent an important amplification of cellular clearance and resolution, severalfold above that which would be achieved by clearance of MSCs alone. Phagocytosis-driven enhancement of resolution is one mechanism by which MSCs may provide protection to distal organs, including the brain. These results represent a novel avenue of translational MSC research and may contribute to the identification of cellular and molecular targets in the immune system and, in turn, improved treatment options in MDD.

ACKNOWLEDGMENTS AND DISCLOSURES

This work was funded by the CReATe Fertility Centre.

We thank Andrea Archila, William Xiao, Beth Pielsticker, and Roberto Lopez for excellent technical support.

CL has filed patent applications in Canada, the United States, and Australia for the invention entitled "Method of Isolation and Use of Cells Derived From First Trimester Umbilical Cord Tissue." The applications have been approved in Australia and Canada and are pending in the United States. CL is also the owner and director of the CReATe Cord Blood Bank and Peristem program and shareholder in Tissue Regeneration Therapeutics (Toronto, Ontario). The other authors report no biomedical financial interests or potential conflicts of interest.

ARTICLE INFORMATION

From the CReATe Fertility Centre (DG, FS, JF, MC, EC, SM, AG-F, CL); Departments of Obstetrics and Gynecology (CL) and Physiology (CL) and Institute of Medical Sciences (CL), University of Toronto; and Department of Gynecology (CL), Women's College Hospital, Toronto, Ontario, Canada.

Address correspondence to Denis Gallagher, Ph.D., 790 Bay Street, Suite 412, Toronto, ON M5G 1N8, Canada; E-mail: denis@createivf.com or gallagher.denisgallagher@gmail.com; or Clifford Librach, M.D., 790 Bay Street, Suite 1100, Toronto, ON M5G 1N8, Canada; E-mail: drlibrach@createivf.com or clifford.librach@sunnybrook.ca.

Received Jan 17, 2019; revised Jul 5, 2019; accepted Jul 15, 2019.

Supplementary material cited in this article is available online at https://doi.org/10.1016/j.biopsych.2019.07.015.

REFERENCES

1. Leday GGR, Vértes PE, Richardson S, Greene JR, Regan T, Khan S, *et al.* (2018): Replicable and coupled changes in innate and adaptive immune gene expression in two case-control studies of blood microarrays in major depressive disorder. Biol Psychiatry 83:70–80.
2. Pfau ML, Menard C, Russo SJ (2017): Inflammatory mediators in mood disorders: Therapeutic opportunities. Annu Rev Pharmacol Toxicol 58:14.1–14.
3. Wium-Andersen MK, Ørsted DD (2013): Elevated C-reactive protein levels, psychological distress, and depression in 73131 individuals. JAMA Psychiatry 70:176–184.
4. Jones KA, Thomsen C (2013): The role of the innate immune system in psychiatric disorders. Mol Cell Neurosci 53:52–62.
5. Valkanova V, Ebmeier KP, Allan CL (2013): CRP, IL-6 and depression: A systematic review and meta-analysis of longitudinal studies. J Affect Disord 150:736–744.
6. Gilman SE, Trinh NH, Smoller JW, Fava M, Murphy JM, Breslau J (2014): Psychosocial stressors and the prognosis of major depression: A test of Axis IV. Psychol Med 43:303–316.
7. Miller AH, Raison CL (2016): The role of inflammation in depression: From evolutionary imperative to modern treatment target. Nat Rev Immunol 16:22–34.
8. McKim DB, Patterson JM, Wohleb ES, Jarrett BL, Reader BF, Godbout JP, *et al.* (2016): Sympathetic release of splenic monocytes promotes recurring anxiety following repeated social defeat. Biol Psychiatry 79:803–813.
9. Wohleb ES, Franklin T, Iwata M, Duman RS (2016): Integrating neuroimmune systems in the neurobiology of depression. Nat Rev Neurosci 17:497–511.
10. Weber MD, Godbout JP, Sheridan JF (2017): Repeated social defeat, neuroinflammation, and behavior: Monocytes carry the signal. Neuropsychopharmacology 42:46–61.
11. Stark JL, Avitsur R, Hunzeker J, Padgett DA, Sheridan JF (2002): Interleukin-6 and the development of social disruption-induced glucocorticoid resistance. J Neuroimmunol 124:9–15.
12. Powell ND, Sloan EK, Bailey MT, Arevalo JMG, Miller GE, Chen E, *et al.* (2013): Social stress up-regulates inflammatory gene expression in the leukocyte transcriptome via β-adrenergic induction of myelopoiesis. Proc Natl Acad Sci U S A 110:16574–16579.
13. Wohleb ES, Powell ND, Godbout JP, Sheridan JF (2013): Stress-induced recruitment of bone marrow-derived monocytes to the brain promotes anxiety-like behavior. J Neurosci 33:13820–13833.

14. Hodes GE, Kana V, Menard C, Merad M, Russo SJ (2015): Neuroimmune mechanisms of depression. Nat Neurosci 18:1386–1393.
15. Ramirez K, Shea DT, McKim DB, Reader BF, Sheridan JF (2015): Imipramine attenuates neuroinflammatory signaling and reverses stress-induced social avoidance. Brain Behav Immun 46:212–220.
16. Bhattacharya A, Drevets WC (2017): Role of neuro-immunological factors in the pathophysiology of mood disorders: Implications for novel therapeutics for treatment resistant depression. Curr Top Behav Neurosci 31:339–356.
17. Fullerton JN, Gilroy DW (2016): Resolution of inflammation: A new therapeutic frontier. Nat Rev Drug Discov 15:551–567.
18. Serhan CN (2017): Treating inflammation and infection in the 21st century: New hints from decoding resolution mediators and mechanisms. FASEB J 31:1273–1288.
19. Ho MSH, Mei SHJ, Stewart DJ (2015): The immunomodulatory and therapeutic effects of mesenchymal stromal cells for acute lung injury and sepsis. J Cell Physiol 230:2606–2617.
20. Le Blanc K, Mougiakakos D (2012): Multipotent mesenchymal stromal cells and the innate immune system. Nat Rev Immunol 12:383–396.
21. Najar M, Raicevic G, Fayyad-Kazan H, Bron D, Toungouz M, Lagneaux L (2016): Mesenchymal stromal cells and immunomodulation: A gathering of regulatory immune cells. Cytotherapy 18:160–171.
22. Gao F, Chiu SM, Motan DAL, Zhang Z, Chen L, Ji HL, *et al.* (2016): Mesenchymal stem cells and immunomodulation: Current status and future prospects. Cell Death Dis 7:e2062.
23. English K, Mahon BP (2011): Allogeneic mesenchymal stem cells: Agents of immune modulation. J Cell Biochem 112:1963–1968.
24. Galipeau J, Sensébé L (2018): Mesenchymal stromal cells: Clinical challenges and therapeutic opportunities. Cell Stem Cell 680:824–833.
25. Trounson A, Mcdonald C (2015): Stem cell therapies in clinical trials: Progress and challenges. Cell Stem Cell 17:11–22.
26. Lee RH, Pulin AA, Seo MJ, Kota DJ, Ylostalo J, Larson BL, *et al.* (2009): Intravenous hMSCs improve myocardial infarction in mice because cells embolized in lung are activated to secrete the anti-inflammatory protein TSG-6. Cell Stem Cell 5:54–63.
27. Eggenhofer E, Benseler V, Kroemer A, Popp FC, Geissler EK, Schlitt HJ, *et al.* (2012): Mesenchymal stem cells are short-lived and do not migrate beyond the lungs after intravenous infusion. Front Immunol 3:1–8.
28. Laroni A, Kerlero N, Rosbo D, Uccelli A (2015): Mesenchymal stem cells for the treatment of neurological diseases: Immunoregulation beyond neuroprotection. Immunol Lett 168:183–190.
29. Caplan AI, Sorrell JM (2015): The MSC curtain that stops the immune system. Immunol Lett 168:136–139.
30. Galleu A, Riffo-Vasquez Y, Trento C, Lomas C, Dolcetti L, Shing T, *et al.* (2017): Apoptosis in mesenchymal stromal cells induces in vivo recipient-mediated immunomodulation. Sci Transl Med 9.
31. de Witte SFH, Luk F, Sierra Parraga JM, Gargesha M, Merino A, Korevaar SS, *et al.* (2018): Immunomodulation by therapeutic mesenchymal stromal cells (MSC) is triggered through phagocytosis of MSC by monocytic cells. Stem Cells 36:602–615.
32. Hong SH, Maghen L, Kenigsberg S, Teichert AM, Rammeloo AW, Shlush E, *et al.* (2013): Ontogeny of human umbilical cord perivascular cells: Molecular and fate potential changes during gestation. Stem Cells Dev 22:2425–2439.
33. Wohleb ES, Hanke ML, Corona AW, Powell ND, Stiner LM, Bailey MT, *et al.* (2011): β-Adrenergic receptor antagonism prevents anxiety-like behavior and microglial reactivity induced by repeated social defeat. J Neurosci 31:6277–6288.
34. McKim DB, Niraula A, Tarr AJ, Wohleb ES, Sheridan JF, Godbout JP (2016): Neuroinflammatory dynamics underlie memory impairments after repeated social defeat. J Neurosci 36:2590–2604.
35. McKim DB, Weber MD, Niraula A, Sawicki CM, Liu X, Jarrett BL, *et al.* (2018): Microglial recruitment of IL-1β-producing monocytes to brain endothelium causes stress-induced anxiety. Mol Psychiatry 23:1421–1431.
36. Soehnlein O, Lindbom L (2010): Phagocyte partnership during the onset and resolution of inflammation. Nat Rev Immunol 10:427–439.
37. Borregaard N (2010): Neutrophils, from marrow to microbes. Immunity 33:657–670.
38. Leal SM Jr, Vareechon C, Cowden S, Cobb BA, Latgé J, Momany M, *et al.* (2012): Fungal antioxidant pathways promote survival against neutrophils during infection. J Clin Invest 122:2482–2498.
39. Bodas M, Mazur S, Min T, Vij N (2018): Inhibition of histone-deacetylase activity rescues inflammatory cystic fibrosis lung disease by modulating innate and adaptive immune responses. Respir Res 19:1–12.
40. Das S, Raundhal M, Chen J, Oriss TB, Huff R, Williams JV, *et al.* (2017): Respiratory syncytial virus infection of newborn CX3CR1-deficient mice induces a pathogenic pulmonary innate immune response. JCI Insight 2.
41. Serhan CN, Savill J (2005): Resolution of inflammation: The beginning programs the end. Nat Immunol 6:1191–1197.
42. Greenlee-Wacker MC (2016): Clearance of apoptotic neutrophils and resolution of inflammation. Immunol Rev 273:357–370.
43. Poon IKH, Lucas CD, Rossi AG, Ravichandran KS (2014): Apoptotic cell clearance: Basic biology and therapeutic potential. Nat Rev Immunol 14:166–180.
44. Kumar KP, Nicholls AJ, Wong CHY (2018): Partners in crime: Neutrophils and monocytes/macrophages in inflammation and disease. Cell Tissue Res 371:551–565.
45. Zhang B, Duan Z, Zhao Y (2009): Mouse models with human immunity and their application in biomedical research. J Cell Mol Med 13:1043–1058.
46. Oberbarnscheidt MH, Zeng Q, Li Q, Dai H, Williams AL, Shlomchik WD, *et al.* (2014): Non-self recognition by monocytes initiates allograft rejection. J Clin Invest 124:3579–3589.
47. Schwartz M, Deczkowska A (2016): Neurological disease as a failure of brain—immune crosstalk: The multiple faces of neuroinflammation. Trends Immunol 37:668–679.
48. Menard C, Pfau ML, Hodes GE, Kana V, Victoria X, Bouchard S, *et al.* (2018): Social stress induces neurovascular pathology promoting depression. Nat Neurosci 20:1752–1760.
49. Kiraly DD, Horn SR, Van Dam NT, Costi S, Schwartz J, Patel M, *et al.* (2017): Altered peripheral immune profiles in treatment-resistant depression: Response to ketamine and prediction of treatment outcome. Transl Psychiatry 7:e1065.
50. Dowlati Y, Herrmann N, Swardfager W, Liu H, Sham L, Reim EK, *et al.* (2010): A meta-analysis of cytokines in major depression. Biol Psychiatry 67:446–457.
51. Zheng X, Ma S, Kang A, Wu M, Wang L, Wang Q, *et al.* (2016): Chemical dampening of Ly6C(hi) monocytes in the periphery produces anti-depressant effects in mice. Sci Rep 6:19406.
52. Mishra SK, Rana P, Khushu S, Gangenahalli G (2017): Therapeutic prospective of infused allogenic cultured mesenchymal stem cells in traumatic brain injury mice: A longitudinal proton magnetic resonance spectroscopy assessment. Stem Cells Transl Med 6:316–329.
53. Tfilin M, Sudai E, Merenlender A, Gispan I, Yadid G, Turgeman G (2010): Mesenchymal stem cells increase hippocampal neurogenesis and counteract depressive-like behavior. Mol Psychiatry 15:1164–1175.
54. Kin K, Yasuhara T, Kameda M, Tomita Y, Umakoshi M, Kuwahara K, *et al.* (2018): Cell encapsulation enhances antidepressant effect of the mesenchymal stem cells and counteracts depressive-like behavior of treatment-resistant depressed rats [published online ahead of print Aug 14]. Mol Psychiatry.
55. Hodes GE, Pfau ML, Leboeuf M, Golden SA, Christoffel DJ, Bregman D, *et al.* (2014): Individual differences in the peripheral immune system promote resilience versus susceptibility to social stress. Proc Natl Acad Sci U S A 111:16136–16141.
56. Ichim TE, Heeron PO, Kesari S (2018): Fibroblasts as a practical alternative to mesenchymal stem cells. J Transl Med 2:1–9.
57. Butovsky O, Ziv Y, Schwartz A, Landa G, Talpalar AE, Pluchino S, *et al.* (2006): Microglia activated by IL-4 or IFN-gamma differentially induce neurogenesis and oligodendrogenesis from adult stem/progenitor cells. Mol Cell Neurosci 31:149–160.